Available on the CERN CDS information server **CMS PAS SUS-16-003**

CMS Physics Analysis Summary

Contact: cms-pag-conveners-susy@cern.ch 2016/03/21

Search for SUSY with multileptons in proton proton collisions at $\sqrt{s} = 13$ TeV

The CMS Collaboration

Abstract

A search for new physics is performed using events with multileptons (≥ 3 electrons or muons) in the final state using the CMS detector. Results are based on a sample of proton-proton collisions at a centre-of-mass energy of 13 TeV at the LHC corresponding to an integrated luminosity of 2.3 fb^{-1}. Search regions have been defined by the number of b-tagged jets, missing transverse energy, hadronic transverse energy, and the invariant mass of opposite-sign, same-flavor dilepton pairs in the events. No excess above the standard model background expectation is observed. In a model with gluino pair production where the gluino decays to two top quarks and a neutralino, gluinos with mass less than 1125 GeV are excluded.

1 Introduction

The multilepton (three or more leptons) final state is a strongly motivated place to search for new physics. The standard model (SM) processes that produce this final state are characterized by having multiple bosons, which are well-understood both theoretically and experimentally. Many different types of beyond the standard model (BSM) theories can produce multilepton events, with a wide array of unique signatures. This analysis is designed to have broad sensitivity to these possibilities by examining the event yields as a function of several kinematic quantities.

This note describes the methods and results of a search for new physics in final states with three or more leptons (electrons or muons) in proton-proton collisions at a center-of-mass energy of 13 TeV at the LHC using the CMS detector with 2.3 fb^{-1} of integrated luminosity. Kinematic regions have been defined to optimize the search for events that contain high jet or b-tagged jet multiplicities. For these final states, the expected irreducible backgrounds come from diboson production ($\text{W}^{\pm}\text{Z}$ and ZZ) or rare SM processes (including $\text{t}\bar{\text{t}}\text{W}^{\pm}$, $\text{t}\bar{\text{t}}\text{Z}$, $\text{t}\bar{\text{t}}\text{H}$, etc.). These backgrounds are modeled using simulation samples that have appropriate corrections applied to match the behavior of reconstructed objects in data. Reducible backgrounds are processes that produce one or more misidentified or nonprompt leptons, i.e. those that come from jets or meson decays, that pass all reconstruction, identification, and isolation criteria. Data driven techniques to measure probabilities of observing misidentified or nonprompt leptons are used to predict the reducible background contributions.

The results of this analysis are interpreted in the context of supersymmetric (SUSY) models that feature strong squark and gluino production with mass spectra that produce final state leptons through the decays of vector bosons. In addition to multiple leptons, these models contain multiple jets and missing transverse energy.

Similar searches have been carried out by CMS using the 8 TeV dataset [1, 2], as well as by ATLAS [3]. Previous searches exclude models with gluino mass less than approximately 1000 GeV (for neutralino mass = 50 GeV). In models featuring bottom squark pair production, the limits are approximately 600 GeV. The present search extends the range of gluino masses excluded by previous searches up to 1125 GeV and excludes bottom squark masses up to 550 GeV.

2 Event selection and Monte Carlo simulation

Events used in this analysis are selected by high-level triggers (HLT) that target di- and multilepton events for offline study. One set of triggers requires that the two leptons meet loose isolation criteria and that the leading lepton has $p_{\text{T}} > 17\,\text{GeV}$ and the sub-leading lepton has $p_{\text{T}} > 8(12)\,\text{GeV}$ in the case of muons (electrons). The second set of triggers places no requirements on the isolation, has a lower p_{T} threshold for the two leptons ($p_{\text{T}} > 8\,\text{GeV}$), and also requires that the hadronic activity reconstructed in the HLT be greater than 300 GeV.

The offline selection requires that there be at least three well-identified leptons in the event and that opposite-sign same-flavor pairs have an invariant mass greater than 12 GeV to reject Drell-Yan and quarkonia processes. The leptons must pass offline p_{T} thresholds of 20, 15, and 10 GeV for the first, second, and third leptons, respectively, when p_{T}-ordered. For this offline selection, the trigger efficiency is above 99%.

Muon candidates are reconstructed combining the information from both the silicon tracker and the muon spectrometer in a global fit [4]. An identification is performed using the quality of the geometrical matching between the tracker and the muon system measurements. To ensure

the candidates are within the fiducial volume of the detector, we require that the candidate pseudorapidity $|\eta| < 2.4$.

Electron candidates are reconstructed using tracking and electromagnetic calorimeter information by combining ECAL superclusters and gaussian sum filter (GSF) tracks [5]. The electron identification is performed using a multivariate discriminant built with shower-shape variables, track-cluster matching variables, and track quality variables. The working point for the selection is chosen to maintain approximately 90% efficiency for accepting electrons produced in the decays of SM bosons and to also efficiently reject candidates originating from jets. To reject electrons originating from photon conversion, electrons are required to have all possible hits in the innermost tracker layers and to not be compatible with any conversion-like secondary vertices. Electrons must have $|\eta| < 2.5$.

Both muon and electron candidates are required to have transverse impact parameter less than 0.5 mm from the event's primary vertex and a longitudinal impact parameter less than 1 mm. In addition, a cut on the 3D impact parameter significance is applied. This variable is the value of impact parameter divided by its uncertainty. This variable should be less than 4 for both electrons and muons. We find that the rejection of nonprompt leptons is much higher using this cut than cuts on the impact parameter that have similar prompt lepton acceptance.

The lepton isolation is constructed using three different variables. The mini isolation, I_{mini}, is the ratio of the amount of energy in a cone with a p_{T}-dependent radius, $R = \frac{10}{\min(\max(p_{\text{T}}(\ell),50),200)}$. Requiring I_{mini} below a given threshold ensures that the lepton is locally isolated, even in boosted topologies.

The second variable is the ratio of the lepton p_{T} and p_{T} of the jet matched to the lepton: $p_{\text{T}}^{\text{ratio}} = \frac{p_{\text{T}}(\ell)}{p_{\text{T}}(\text{jet})}$. This jet is matched geometrically to the lepton and residing within $\Delta R < 0.4$ from it. In most of the cases, this is the jet containing the lepton. If no jet within $\Delta R < 0.4$ is found then lepton itself is used to compute $p_{\text{T}}^{\text{ratio}} = 1$. The use of $p_{\text{T}}^{\text{ratio}}$ is a simple way to identify non-prompt low-p_{T} leptons originating from low-p_{T} b-quarks which decay with larger aperture than the one used in mini isolation.

The last variable used is the $p_{\text{T}}^{\text{rel}}$ variable, which is calculated by subtracting the lepton from the momentum vector of the geometrically matched jet described above and then finding the component of the lepton momentum which is transverse to this new vector. This variable allows us to recover leptons from accidental overlap with jets in boosted topologies.

Using those three variables, a lepton is considered isolated if the following condition is respected:

$$I_{\text{mini}} < I_1 \&\& (p_{\text{T}}^{\text{ratio}} > I_2 || p_{\text{T}}^{\text{rel}} > I_3) \quad (1)$$

The $I_i, i = 1,2,3$ values depend of the flavor of the lepton: as the probability to misidentify a jet is higher for the electrons, tighter isolation values are used. The logic behind this isolation is that a lepton should be locally isolated (I_{mini}), carry the major part of the energy of the corresponding jet ($p_{\text{T}}^{\text{ratio}}$), or if not, then this lepton is accepted if its overlap with a jet is accidental ($p_{\text{T}}^{\text{rel}}$). The loose lepton isolation is significantly relaxed: $I_{\text{mini}} < 0.4$ while the other requirements are dropped. For muons (electrons), the tight selection requirements are $I_1 = 0.16(0.12)$, $I_2 = 0.69(0.76)$, and $I_3 = 6.0(7.2)$.

Jets are reconstructed from particle flow candidates [6], clustered with the anti-k_{T} algorithm and with a distance parameter of $R = 0.4$. Only jets above a transverse momentum $p_{\text{T}} > 30\,\text{GeV}$ and within the tracker acceptance $|\eta| < 2.4$ are considered. Additional criteria are applied to reject events containing noise and mismeasured jets. To avoid double counting due to jets

matched geometrically with a lepton, the jet the closest matched to a lepton is not considered as a jet in the event, if the jet is within a cone of $\Delta R < 0.4$. From those selected jets, the key variable H_{T} is defined by $H_{\mathrm{T}} = \sum_{jets} p_{\mathrm{T}}$, where the sum runs over all jets which satisfy the above mentioned criteria.

A combined secondary vertex algorithm [7, 8] is used to assess the likelihood that a jet originates from a bottom quark. Jets in this analysis are considered b-tagged if they pass the algorithm's medium working point, which has a tagging efficiency of 70% and a mistag rate of 1%.

The missing transverse energy $E_{\mathrm{T}}^{\mathrm{miss}}$ is defined as the magnitude of the negative vector sum of all particle flow candidates reconstructed in an event. The jet energy corrections are propagated to the $E_{\mathrm{T}}^{\mathrm{miss}}$ following the procedure described in [9].

To estimate the contribution of the SM processes to our signal regions and to calculate the efficiency for new physics models, Monte Carlo (MC) simulations are used. For the SM samples, the MADGRAPH _MC@NLO [10] and POWHEG [11] programs are used for event generation at leading order (LO) or next-to-leading order (NLO) in perturbative QCD. Parton showering and hadronization are simulated using PYTHIA 8 [12]. The CMS detector response is determined using a GEANT 4-based model [13].

The production processes of SUSY signal samples are generated with MADGRAPH _MC@NLO at LO precision, with an allowance for up to two additional partons in the matrix element calculations. The SUSY particle decays, parton showering, and hadronization are simulated in PYTHIA 8. The detector response for signal events is simulated using a CMS fast-simulation package [14] that is validated against the GEANT 4-based model. All simulated events are processed with the same reconstruction procedure as data. Corrections are applied so that the distribution of interactions per bunch crossing are the same in the simulation as in data. Cross sections for SUSY signal processes, calculated at NLO with next-to-leading-log (NLL) resummation, are taken from the LHC SUSY Cross Sections Working Group [15–19].

3 Search strategy

The goal of this analysis is to search for possible excesses over the expected yields from the SM processes in events with three or more leptons. With 2.3 fb^{-1} available data at 13 TeV, the search is focused on the strongly produced SUSY particles which benefit the most from the rise in the production cross section. A few example SUSY processes which can give rise to multilepton final states are shown in Fig. 1. The models in Figures 1a, 1b, and 1c are simplified model spectra (SMS). In these models, SUSY particles that are not directly included in the diagrams are forced to be too heavy to be accessible at the LHC. Therefore, the free parameters in these models is usually the mass of the produced particle, gluinos and squarks in these cases, and the mass of the lightest super partner (LSP).

A typical process within SUSY includes the one known as T1tttt: gluino-pair production where each gluino decays to a $\mathrm{t\bar{t}}$ pair and an LSP (Fig. 1a). Another model containing gluino-pair production where each gluino decays to a pair of quarks and a neutralino or chargino and that neutralino or chargino then decays to a W or Z boson and an LSP, depending on the charge, is called T5qqqqWZ (Fig. 1b). A model called T6ttWW, features 3$^{\mathrm{rd}}$ generation squark-pair production with their subsequent cascade decays via top-quarks and W/Z/H-bosons (Fig. 1c). The LSP is a neutralino in all of the considered models.

For the definition of the signal regions we use several event variables: number of b-jets ($N_{\mathrm{b\,jets}}$),

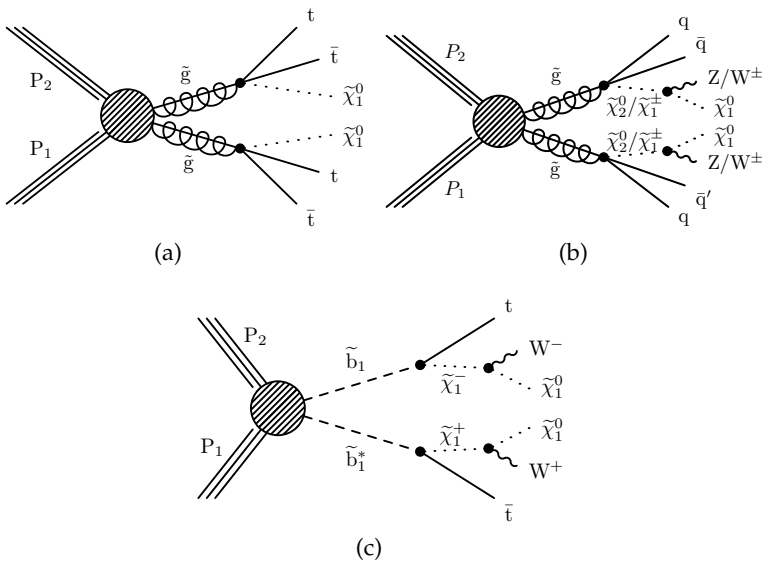

Figure 1: Diagrams for gluino and bottom squark pair production which can produce multilepton events: T1tttt (a), T5qqqqWZ (b), and T6ttWW (c).

the hadronic activity (H_T), the missing transverse energy (E_T^{miss}), and whether the event contains any opposite-sign, same-flavor dilepton pairs with an invariant mass between 76 and 106 GeV (on-Z if so, off-Z otherwise).

The separation in b-jet multiplicities ensures the maximization of the signal-to-background ratios for events from different signal models. For example, the T1tttt model features several b-jets, which would be categorized into signal regions which are almost free of WZ background owing to the b-jet requirement. Including the 0 b-tag signal regions keeps the analysis sensitive to signatures without b-jets like the T5qqqqWZ model. Additionally, a categorization in H_T and E_T^{miss} is useful to distinguish between compressed and non-compressed SUSY spectra, i.e. models with small or large mass differences between the SUSY particles in the decay chain.

A baseline selection is applied to the dataset to select events of interest: three or more electrons or muons fulfilling $p_T \geq 20/15/10\,\text{GeV}$, $m_{\ell\ell} \geq 12\,\text{GeV}$, $N_{\text{jets}} \geq 2$, $H_T \geq 60$, $N_{\text{b jets}} \geq 2$, and $E_T^{miss} \geq 50\,\text{GeV}$. Table 1 shows the definition of the subdivision of the baseline selection into 15 signal regions (SR) each for events that contain on-Z and off-Z dilepton pairs. A set of four SR with low or medium H_T and low or medium E_T^{miss} have been defined for each of the b-tag multiplicities 0, 1, and 2. Motivated by the low expected yield of events with 3 or more $N_{\text{b jets}}$, one inclusive SR with $E_T^{miss} < 300$ and $H_T < 600$ has been defined for high b-tag multiplicities ≥ 3 (SR 13). Two additional SR with ultra high H_T (SR 14) and ultra high E_T^{miss} (SR 15) respectively have been defined as nearly background free SRs since various non-compressed SUSY model can yield events with very high E_T^{miss} or H_T. Both of them are inclusive in the number of b-jets and priority is given to ultra high E_T^{miss} region SR 15, meaning that every selected event with $E_T^{miss} \geq 300$ is categorized in this region, while the ultra high H_T region 14 is populated with events with $E_T^{miss} < 300\,\text{GeV}$ and $H_T \geq 600\,\text{GeV}$.

4 Background Estimation

Backgrounds for the multilepton final state can be divided in three categories:

Table 1: multilepton signal region definition

N_{jets}	$N_{\text{b jets}}$	$E_{\text{T}}^{\text{miss}}$ (GeV)	$60\,\text{GeV} \leq H_{\text{T}} < 400\,\text{GeV}$	$400\,\text{GeV} \leq H_{\text{T}} < 600\,\text{GeV}$	$H_{\text{T}} \geq 600\,\text{GeV}$
≥ 2	0	$50-150$	SR1	SR3	SR14
		$150-300$	SR2	SR4	
	1	$50-150$	SR5	SR7	
		$150-300$	SR6	SR8	
	2	$50-150$	SR9	SR11	
		$150-300$	SR10	SR12	
	≥ 3	$50-300$	SR13		
	inclusive	≥ 300	SR15		

- **Nonprompt leptons:** *Nonprompt* or *misidentified* leptons are leptons from heavy-flavour decays, misidentified hadrons, muons from light-meson decays in flight, or electrons from unidentified photon conversions. For this analysis $\mathrm{t\bar{t}}$ events can enter the signal regions if nonprompt leptons are present in addition to the prompt leptons from the W decays. The $\mathrm{t\bar{t}}$ events show typically low H_{T} and $E_{\text{T}}^{\text{miss}}$ and therefore predominately populate the signal regions 1 and 5, with 0 and 1 b-tagged jet respectively. Apart from $\mathrm{t\bar{t}}$, Drell-Yan events can enter the baseline selection, however they are largely suppressed by the $E_{\text{T}}^{\text{miss}} > 50\,\text{GeV}$ cut. Processes which yield only one prompt lepton in addition to non-prompt ones like W+jets and various single top channels are effectively suppressed by the three lepton requirement because of the low probability that two non-prompt leptons pass the tight identification and isolation requirements.
- **Diboson production:** Diboson production could yield multilepton final states with up to three prompt leptons in WZ prompt leptons and up to four prompt leptons in ZZ production, being therefore an irreducible background. Especially in signal regions without b-tagged jets, WZ production has a sizable contribution. To estimate this background, its yield as obtained from simulation is scaled using a scale factor measured in a dedicated control region enriched in WZ events.
- **Rare SM processes:** Other rare SM processes that can yield three or more leptons are $\mathrm{t\bar{t}W}$, $\mathrm{t\bar{t}Z}$, and tri-boson production VVV where V= W, Z. We also include the contribution from the SM Higgs boson produced in association with a vector boson or a pair of top quarks in this category of backgrounds, as well as processes that produce additional leptons from internal conversions, which are events that contain a virtual photon that decays to leptons. The internal conversion background components, X+γ, where X is predominantly $\mathrm{t\bar{t}}$ or Z, are heavily suppressed by the $E_{\text{T}}^{\text{miss}} > 50\,\text{GeV}$ and $N_{\text{jets}} \geq 2$ cuts. Those rare backgrounds are obtained from simulation and appropriate systematic uncertainties are assigned.

The background contribution from nonprompt and misidentified leptons is estimated using the tight-to-loose ratio method. In this method, an application region made up of events that contain at least one of the leptons failing the full set of tight identification and isolation requirements but passing the loose requirements is weighted by $f/(1-f)$, where the tight-to-loose ratio f is the probability that a loosely identified nonprompt lepton also passes the full set of requirements. This ratio is measured as a function of lepton p_{T} and η in a control sample of QCD multijet events that is enriched in nonprompt leptons (measurement region). Exactly one lepton passing the loose object selection is required in the event. Additionally, one recoiling jet with $\Delta R(\text{jet}, \ell) > 1.0$ and low $E_{\text{T}}^{\text{miss}}$ and M_{T}, both $< 20\,\text{GeV}$ are required to suppress events with leptons from W and Z decays, where M_{T} is the transverse mass of the lepton and the $E_{\text{T}}^{\text{miss}}$ vector. The remaining contribution from these electroweak processes within the measurement

region is subtracted using estimates from MC simulations.

The main advance in the development of this method has been to reduce the dependence of the tight-to-loose ratio on the flavor content of the jet from which the nonprompt lepton originates, by parameterizing the ratio as a function of the a variable that correlates more strongly with mother parton p_{T} than the lepton p_{T}. This variable is calculated by correcting the lepton p_{T} as a function of the energy in the isolation cone around it. This definition leaves the p_{T} of the leptons passing the isolation cut unchanged and modifies the p_{T} of those failing the cut so that it is a better proxy for the mother parton p_{T} and results in a flatter ratio as a function of the mother parton p_{T}. The cone correction significantly improves the results of the method when applying it in simulation. The flavor dependence, which is much more important for the case of electrons, is also reduced by adjusting the loose object selection to obtain similar ratios for nonprompt electrons that originate from both light- and heavy-flavor jets.

The tight-to-loose ratio method of estimating the nonprompt background is validated in a control region exclusive to our baseline selection with minimal signal contamination. This region is defined by having three leptons pass nominal identification, isolation cuts and p_{T} requirement, one or two jets, $20 < E_{\mathrm{T}}^{\mathrm{miss}} < 50$ GeV, and no on-Z dilepton pair. We find agreement of the order of 20% between the predicted and observed yields in this control region.

The WZ process is one of the main backgrounds in the regions with 0 b-tags. The estimates for this process are taking from MC simulation, but the normalization is taken from a control region that is highly enriched for this process: three leptons pass nominal identification and isolation cuts, two leptons form a OS, SF pair with $|m_{\ell\ell} - m_{\mathrm{Z}}| < 15$ GeV, the number of jets is zero or one, the number of b-tagged jets is zero, $30\,\mathrm{GeV} < E_{\mathrm{T}}^{\mathrm{miss}} < 100\,\mathrm{GeV}$, the transverse mass of the third lepton (not in the pair forming the Z) is required to be at least 50 GeV to suppress contamination from Drell-Yan process. The purity of WZ in the selected sample is 84%. In this control region, we measure the scale factor on the WZ simulation needed to match the background predictions and the observation in data. The statistical uncertainties on the scale factor are used as additional uncertainties on the WZ prediction in the SRs. The scale factor obtained with 2.3 fb^{-1} of data is 1.13 ± 0.17.

5 Systematic Uncertainties

The different uncertainties are categorized as experimental, as those related to the jet-energy scale or the b-tagging efficiency; theoretical, such as the uncertainties on the considered cross sections; statistical, due to the limited size of the Monte Carlo samples; and uncertainties on the applied data-driven methods. These effects and their magnitudes are described below, and are summarized in Table 2.

The major experimental source of uncertainty is the knowledge of the jet energy scale (JES), affecting all the simulated backgrounds and signal events, which accounts for differences between data and simulation. For the dataset used in this analysis, the uncertainties on the jet energy scale vary from 2% to 8%, depending of the transverse momentum and pseudorapidity of the jet. The impact of this uncertainties is assessed by shifting the jet energy correction factors for each jet up and down by $\pm 1\sigma$ and recalculating all of the kinematic quantities. The JES uncertainties are propagated to the missing transverse energy and all variables derived from jets (number of jets, H_{T}, number of b-jets) used in this analysis. The propagation of the JES uncertainties results in 1–20% variation in the event yields in the most populated SRs.

A similar approach is used for the uncertainties associated with the corrections for the b-

tagging efficiencies for light and bottom flavour jets, which are parametrized as a function of p_T and η. The variation of the scale factor correcting for differences between data and simulation is at maximum of the order of 5–10% per jet, and leads to an overall effect in the range of 1–20% depending on the signal region and on the topology of the events under study. If considering only highly populated signal regions to get an overview of the main effects on the background yields, the bulk of the $t\bar{t}W$ yield varies by $\sim$10% and the WZ yield by $\sim$13%.

Lepton identification scale factors have been measured by comparing efficiencies in data and simulation and are applied as a function of lepton p_T and η. The corresponding uncertainties have been evaluated and are of the order of 2% per lepton for both flavors. Trigger efficiency scale factors have been found to be very close to unity and are neglected. However, a conservative flat uncertainties of 3% is taken into account.

All these uncertainties, related to corrections of the simulation (JES corrections, b-tagging efficiency scale-factors, lepton identification scale-factors) have been estimated also for the fast-simulation used for the signal samples scans. We propagate them to the expected signal yields following the same procedure.

The uncertainty on the QCD renormalization (μ_R) and factorization scales (μ_F), and on the knowledge of the Parton Density Functions (PDF) are considered for some of the rare processes, namely $t\bar{t}H$, $t\bar{t}Z$, and $t\bar{t}H$. Both the changes in acceptance and cross sections due to those effects are taken into account.

For the study of the renormalization and factorization uncertainties, fluctuations up and down by a factor of two with respect to the nominal values of μ_F and μ_R are considered. The maximum difference in the yields with respect to the nominal case is observed when both scales are varied simultaneously up and down. The effect on the overall cross section is found to be $\sim$ 13% for $t\bar{t}W$ and $\sim$ 11% for $t\bar{t}Z$. An additional uncorrelated uncertainty on the acceptance corresponding to different signal regions is included. This is found to be between 3% and 18% depending on the search region and process.

The uncertainty related to the PDF is estimated from the the 100 NNPDF 3.0 replicas, com-

source	magnitude	effect on yield	induces SR migration
luminosity	4.6%	4.6% *	–
jet ES	$2-8\%$	$1-20\%$ *	✓
b-tag efficiency	$5-10\%$	$1-20\%$ *	–
pileup	5%	3% *	–
lepton efficiencies	2%	2% *	–
HLT efficiencies	3%	3% *	–
HLT lepton effic.	$3-10\%$	$3-10\%$ FastSim signals	–
HLT FastSim	5%	5% FastSim signals	–
FO CR stat.	$1-100\%$	$1-100\%$ (fake bkg. only)	–
FR extrapolation	30%	30% (fake bkg. only)	–
EWK subtraction in FR	100% (ewk. SF)	$1-5\%$ (fake bkg. only)	–
WZ CR stat. and norm.	15%	15 % (WZ only)	–
MonteCarlo stat.	$1-100\%$	$1-100\%$ *	–
QCD scales	$\times 0.5/\times 2$	$11-13\%(\sigma)/3-18\%(\mathcal{A})$ ($t\bar{t}W$,$t\bar{t}Z$,$t\bar{t}H$)	–
PDFs	–	2–3% ($t\bar{t}W$,$t\bar{t}Z$,$t\bar{t}H$)	–
other bkgs.	50%	50% (rare processes, tribosons, etc.)	–

* $t\bar{t}W$,$t\bar{t}Z$,$t\bar{t}H$, rare processes and signals only

Table 2: Summary of the sources of uncertainties, their magnitude and their effects. The second column indicates the magnitude of the yield variation. The third column indicates if the source of the uncertainty implies a signal region to signal region migration.

puting the deviation with respect to the nominal yields for each of them, and for each signal regions (the cross section and acceptance effect are considered together) [20]. The root mean square of the variations is taken as the value of the systematic uncertainty. Since no significant fluctuations among the different signal regions are seen, a flat uncertainty of 3% (2%) is applied for $t\bar{t}W$ ($t\bar{t}Z$). This value also includes the effect on $\alpha_S(M_Z)$, which is added in quadrature, and whose magnitude is similar or smaller to such of the PDF set uncertainty. For the $t\bar{t}H$ process, the same uncertainties estimated for $t\bar{t}Z$ are applied. A conservative 50% of theoretical uncertainty is assigned to the remaining rare processes.

In signal samples, an uncertainty for initial state radiation is computed as a function of the p_T of the gluino-gluino system. For values below 400 GeV no uncertainty is applied, for values between 400 and 600 GeV a 15% uncertainty is assigned, while a 30% uncertainty is considered for values above 600 GeV.

The limited size of the generated Monte Carlo samples represents an additional source of uncertainty. For the backgrounds that are estimated from the simulation, like $t\bar{t}W$, $t\bar{t}Z$ and $t\bar{t}H$, as well as for all the signal processes, these uncertainty is computed from the number of Monte-Carlo events entering in each of the signal regions.

For the nonprompt and misidentified lepton background, we assign several systematic uncertainties. The statistical uncertainty from the application region which we use to estimate this background contribution is from 1% to 100%. The regions where these uncertainties are large are generally regions where the overall contribution of this background is small. In the case where no events are observed in the application region, the upper limit of the background expectation is found by applying the most probable value of the tight-to-loose ratio to a Poisson fluctuation.

The systematic uncertainties related to the extrapolation from the control regions to the signal regions for the nonprompt lepton background is estimated to be 30%. This magnitude has been extracted from the level of closure achieved in test which was performed with Monte Carlo samples yielding non-prompt leptons to validate the data-driven background prediction described in Section 4.

The uncertainty associated to the electroweak subtraction in the tight-to-loose ratio computation is propagated along the full analysis process, by replacing the nominal tight-to-loose ratio with another value obtained when the scale factor applied to the electroweak processes in the measurement region is varied by 100%. The overall effect on the nonprompt background yield lies between 1% and 5% depending on the signal region considered.

The estimation of the WZ background gets a 15% normalization uncertainty from the statistical uncertainty in the scale factor measured in a control region. Additional uncertainties for the extrapolation from the control region to the signal regions of 10% – 30% are taken into account depending on the signal region.

6 Results

A detailed summary of predicted event yields for the background processes and the number of observed yields in all the SRs are summarized in Tables 3 and 4 for the off-Z and on-Z regions, respectively. Expected event yields for a few representative signal models is provided in Tables 5 and 6 along with total predicted background and observed events. Comparisons of distributions of H_{T}, $E_{\mathrm{T}}^{\mathrm{miss}}$, N_{jets}, $N_{\mathrm{b\,jets}}$, leading lepton p_{T}, subleading lepton p_{T}, and trailing lepton p_{T} measured in data with those predicted by the background methods are shown in

Fig. 2a-2g (Fig. 3a-3g) , using all the events satisfying the off-Z (on-Z) search region selection criteria. The hatched band represents the total background uncertainty in each bin. Finally, Fig. 2h and Fig. 3h graphically present a summary of predicted backgrounds and observed event yields in individual SRs.

Table 3: The yields for each background source in the off-Z search regions with the 2.3 fb^{-1} of data. For the nonprompt background, the uncertainties are first statistical, then systematic. For the other backgrounds, the uncertainties are systematic, though this includes statistical uncertainties on the simulation samples.

SR	$\bar{t}tW$	$\bar{t}tZ/H$	$X\gamma$	WZ	rare	nonprompt	total	observed
SR1	0.60 ± 0.18	1.10 ± 0.22	$0.51^{+0.56}_{-0.51}$	3.99 ± 0.83	0.62 ± 0.20	$12.44 \pm 2.84 \pm 3.73$	$19.26^{+4.81}_{-4.80}$	18
SR2	0.11 ± 0.06	0.24 ± 0.07	$0.01^{+0.24}_{-0.01}$	0.60 ± 0.15	0.13 ± 0.05	$0.07^{+0.16}_{-0.06}$	$1.16^{+0.31}_{-0.20}$	4
SR3	0.05 ± 0.04	0.18 ± 0.06	$0.01^{+0.25}_{-0.01}$	0.25 ± 0.07	0.07 ± 0.03	$0.64 \pm 0.32 \pm 0.19$	$1.20^{+0.47}_{-0.40}$	3
SR4	$0.01^{+0.03}_{-0.01}$	0.07 ± 0.03	$0.01^{+0.25}_{-0.01}$	0.17 ± 0.06	0.02 ± 0.02	$0.00^{+0.35}_{-0.00}$	$0.29^{+0.44}_{-0.09}$	0
SR5	1.04 ± 0.29	2.03 ± 0.39	0.71 ± 0.47	0.22 ± 0.07	0.21 ± 0.07	$12.37 \pm 2.48 \pm 3.71$	16.57 ± 4.52	24
SR6	0.27 ± 0.10	0.38 ± 0.08	$0.00^{+0.26}_{-0.00}$	0.05 ± 0.03	0.02 ± 0.01	$1.61 \pm 0.57 \pm 0.48$	$2.32^{+0.80}_{-0.76}$	1
SR7	0.17 ± 0.07	0.45 ± 0.10	$0.01^{+0.26}_{-0.01}$	0.02 ± 0.01	0.03 ± 0.01	$0.00^{+0.35}_{-0.00}$	$0.67^{+0.45}_{-0.09}$	2
SR8	0.15 ± 0.06	0.15 ± 0.05	$0.04^{+0.25}_{-0.04}$	0.03 ± 0.02	0.02 ± 0.01	$0.08^{+0.13}_{-0.08}$	$0.48^{+0.29}_{-0.07}$	0
SR9	0.65 ± 0.18	0.80 ± 0.16	$0.07^{+0.27}_{-0.07}$	0.00 ± 0.00	0.06 ± 0.02	$2.91 \pm 1.54 \pm 0.87$	$4.49^{+1.81}_{-1.79}$	4
SR10	0.11 ± 0.05	0.14 ± 0.04	$0.05^{+0.26}_{-0.05}$	$0.00^{+0.01}_{-0.00}$	0.01 ± 0.01	$0.00^{+0.35}_{-0.00}$	$0.31^{+0.44}_{-0.09}$	1
SR11	0.11 ± 0.05	0.30 ± 0.07	$0.01^{+0.26}_{-0.01}$	$0.00^{+0.01}_{-0.00}$	0.02 ± 0.01	$0.00^{+0.04}_{-0.00}$	$0.40^{+0.27}_{-0.26}$	0
SR12	0.04 ± 0.03	0.04 ± 0.03	$0.00^{+0.25}_{-0.00}$	$0.00^{+0.01}_{-0.00}$	0.01 ± 0.01	$0.00^{+0.35}_{-0.00}$	$0.08^{+0.43}_{-0.08}$	0
SR13	0.01 ± 0.01	0.07 ± 0.02	$0.03^{+0.25}_{-0.03}$	$0.00^{+0.01}_{-0.00}$	0.02 ± 0.01	$0.00^{+0.35}_{-0.00}$	$0.13^{+0.43}_{-0.09}$	0
SR14	0.32 ± 0.11	0.57 ± 0.13	$0.14^{+0.27}_{-0.14}$	0.23 ± 0.07	0.17 ± 0.06	$0.42 \pm 0.25 \pm 0.13$	$1.84^{+0.44}_{-0.37}$	3
SR15	0.05 ± 0.05	0.07 ± 0.04	$0.02^{+0.25}_{-0.02}$	0.13 ± 0.05	0.04 ± 0.01	$1.31 \pm 1.12 \pm 0.39$	$1.62^{+1.22}_{-1.19}$	0

The number of events observed in data are found to be consistent with predicted background yields. The results are used to calculate cross section upper limits on production of gluinos or squarks for various models discussed in Section 3 as a function of the gluino or squark and the chargino or neutralino masses. For each mass point, the observation, background predictions, and expected signal yields from all onZ and offZ search regions are combined to extract a cross section that can be excluded at a 95% confidence level (CL) using the LHC-type CL_s method. Log-normal nuisance parameters are used to describe the systematic uncertainties listed in Section 5.

The results of the limit setting procedure are shown in Figures 4 to 6 for the considered simplified models. In these figures, the thick black lines delineate the observed exclusion region, which is to the left of the line. The uncertainty on the observed limit, represented by the thinner black lines, is the propagation the of the cross section uncertainties for the relevant signal process. The red dashed lines represent the expected limits with uncertainties reflecting those discussed in Section 5.

7 Conclusions

We have presented the analysis strategy to search for beyond the standard model physics in final states with ≥ 3 leptons, electrons or muons, using 2.3 fb^{-1} collected using the CMS detector at $\sqrt{s} = 13\,\text{TeV}$. The analysis makes use of data-driven techniques to estimate reducible back-

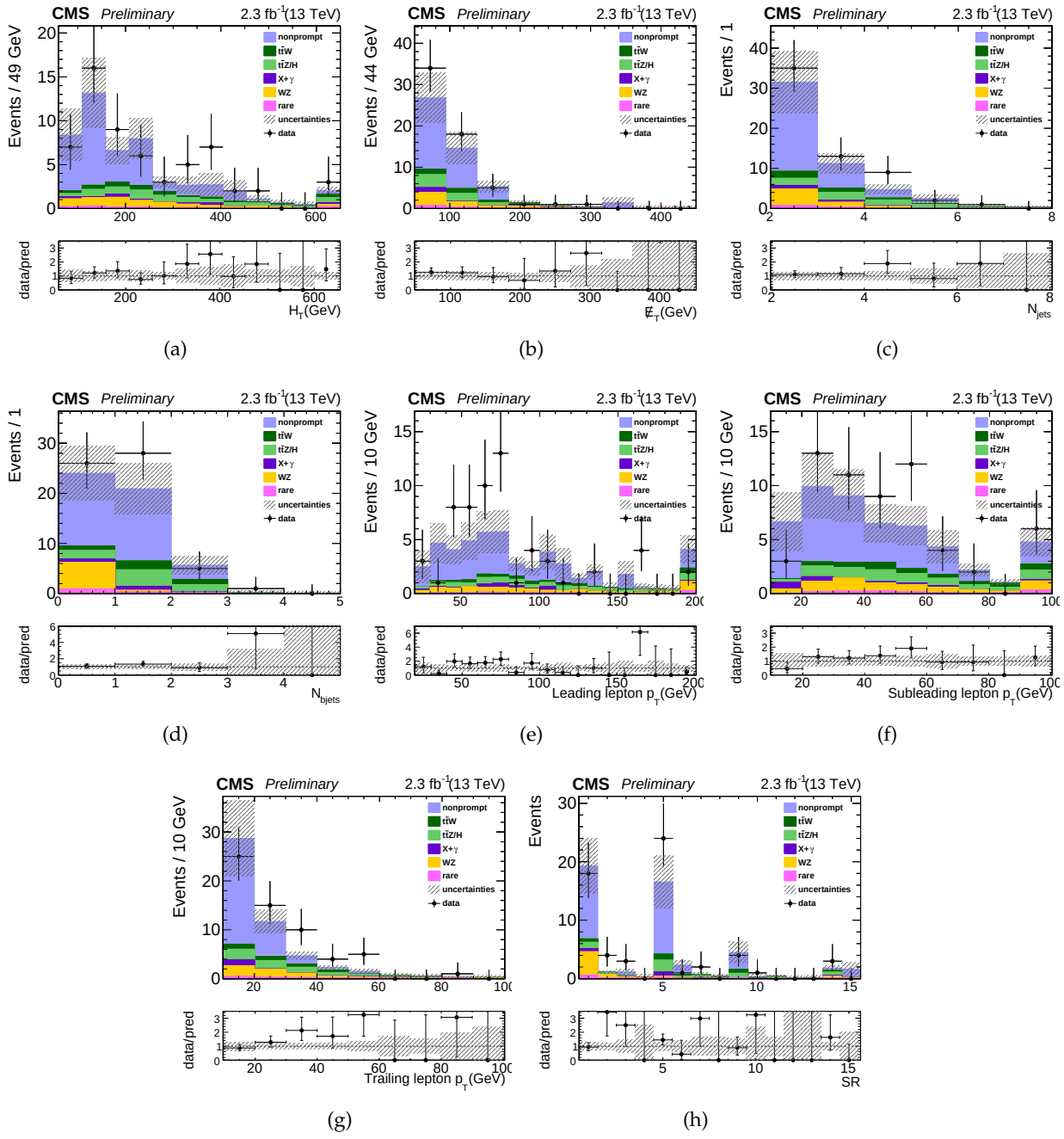

Figure 2: Comparisons of the distributions of (a) H_{T}, (b) $E_{\mathrm{T}}^{\mathrm{miss}}$, (c) N_{jets}, (d) $N_{\mathrm{b\,jets}}$, (e-g) p_{T} of leptons for the background predictions to those observed in data in the off-Z baseline selection region. The nonprompt lepton backgrounds come from the data-driven technique described in Section 4. The total predicted background and number of events observed in 15 off-Z SRs is shown in (h).

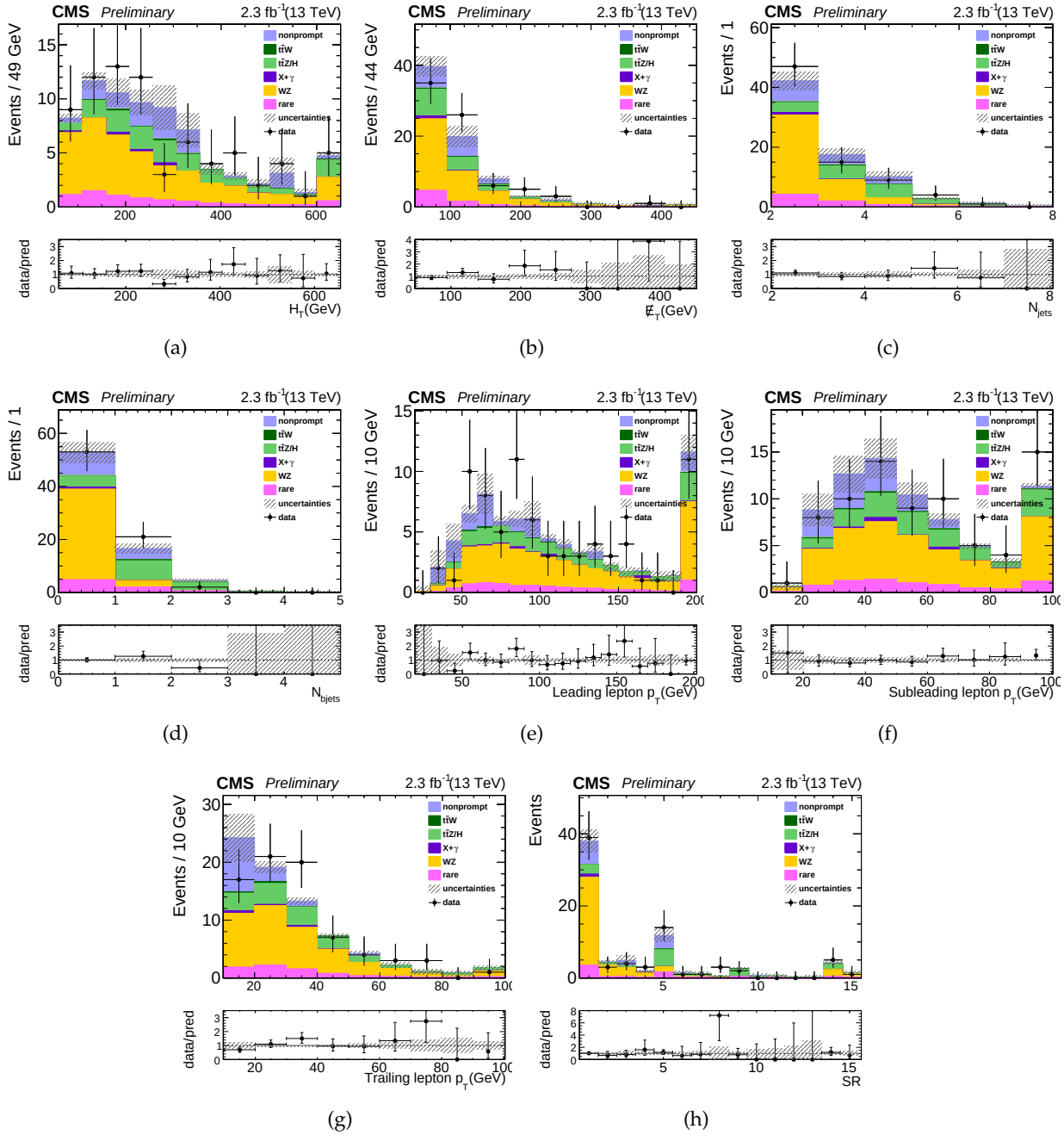

Figure 3: Comparisons of the distributions of (a) H_{T}, (b) $E_{\mathrm{T}}^{\mathrm{miss}}$, (c) N_{jets}, (d) $N_{\mathrm{b\,jets}}$, (e-g) p_{T} of leptons for the background predictions to those observed in data in the on-Z baseline selection region. The nonprompt lepton backgrounds come from the data-driven technique described in Section 4. The total predicted background and number of events observed in 15 on-Z SRs is shown in (h).

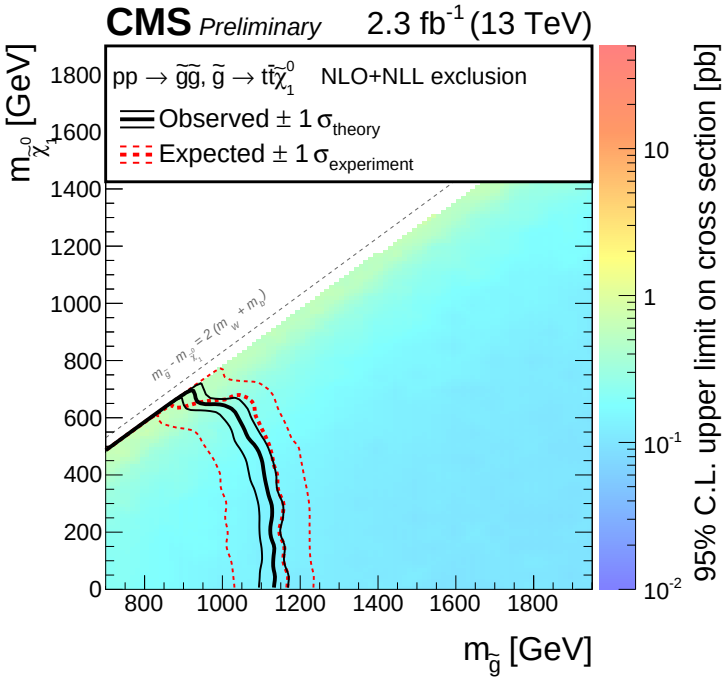

Figure 4: Excluded region at 95% confidence in the $m(\widetilde{\chi}^0)$ versus $m(\widetilde{g})$ plane for the T1tttt simplified model. The color scale indicates the excluded cross section at a given point in the mass plane. The excluded regions are to the left and below the observed and expected limit curves.

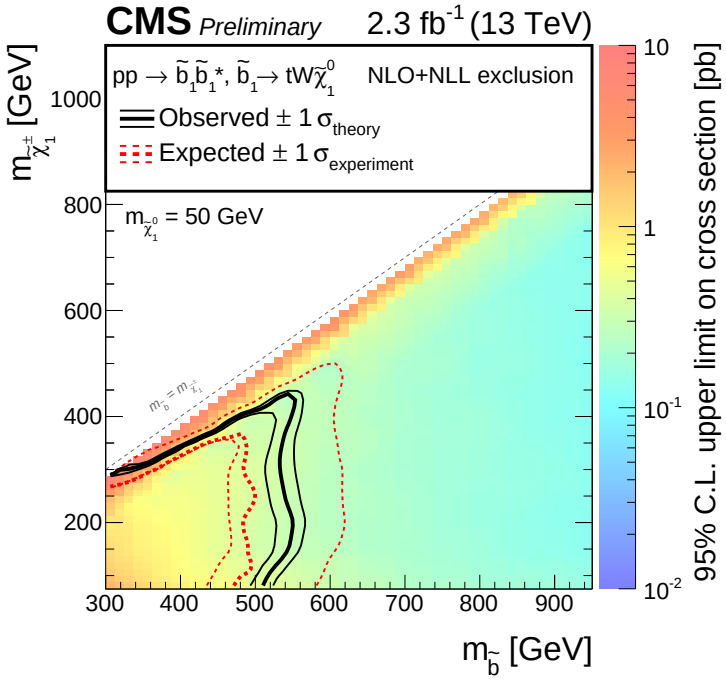

Figure 5: Excluded region at 95% confidence in the $m(\widetilde{\chi}^{\pm})$ versus $m(\widetilde{b})$ plane for the T6ttWW simplified model. The color scale indicates the excluded cross section at a given point in the mass plane. The excluded regions are to the left and below the observed and expected limit curves.

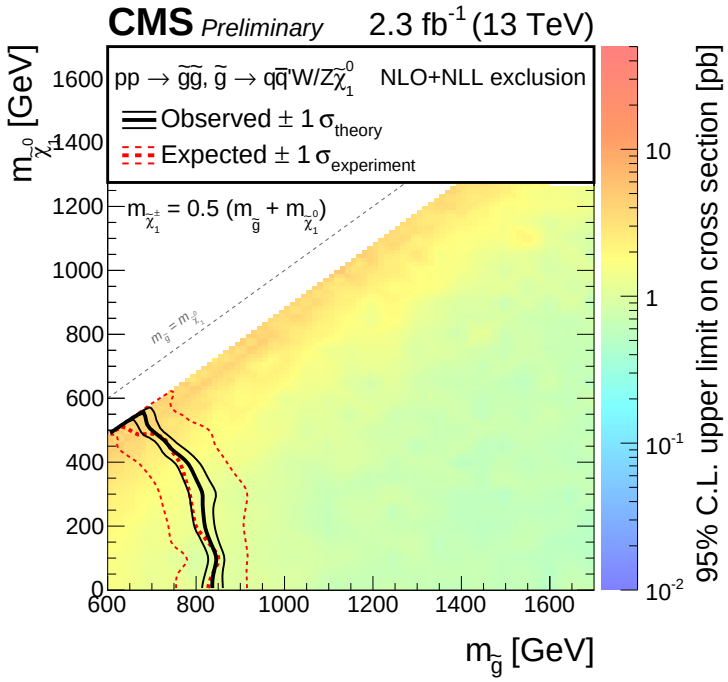

Figure 6: Excluded region at 95% confidence in the $m(\tilde{\chi}^0)$ versus $m(\tilde{g})$ plane for the T5qqqqWZ simplified model. For this model the WW final state has been filtered out and the gluino-gluino cross section has been scaled down accordingly. The ZZ final state is neglected because of the low leptonic branching ratio. The color scale indicates the excluded cross section at a given point in the mass plane. The excluded regions are to the left and below the observed and expected limit curves.

Table 4: The yields for each background source in the on-Z search regions with the 2.3 fb^{-1} of data. For the nonprompt background, the uncertainties are first statistical, then systematic. For the other backgrounds, the uncertainties are systematic, though this includes statistical uncertainties on the simulation samples.

SR	$t\bar{t}W$	$t\bar{t}Z/H$	$X\gamma$	WZ	rare	nonprompt	total	observed
SR1	0.12 ± 0.05	2.67 ± 0.67	0.80 ± 0.57	24.50 ± 4.93	3.48 ± 0.88	$6.44 \pm 2.32 \pm 1.93$	38.01 ± 5.92	39
SR2	0.04 ± 0.02	0.58 ± 0.17	$0.02^{+0.25}_{-0.02}$	3.27 ± 0.68	0.35 ± 0.10	$0.23^{+0.36}_{-0.23}$	$4.48^{+0.84}_{-0.75}$	3
SR3	0.04 ± 0.02	0.47 ± 0.15	$0.00^{+0.25}_{-0.00}$	2.46 ± 0.52	0.37 ± 0.10	$1.56 \pm 1.28 \pm 0.47$	$4.88^{+1.49}_{-1.47}$	4
SR4	$0.00^{+0.02}_{-0.00}$	0.04 ± 0.04	$0.01^{+0.25}_{-0.01}$	1.37 ± 0.30	0.13 ± 0.04	$0.31 \pm 0.23 \pm 0.09$	$1.88^{+0.47}_{-0.39}$	3
SR5	0.24 ± 0.09	4.61 ± 1.13	$0.06^{+0.25}_{-0.06}$	1.53 ± 0.33	1.57 ± 0.66	$3.81 \pm 1.42 \pm 1.14$	$11.84^{+2.28}_{-2.26}$	14
SR6	0.08 ± 0.04	0.72 ± 0.20	$0.00^{+0.25}_{-0.00}$	0.30 ± 0.09	0.12 ± 0.05	$0.30 \pm 0.22 \pm 0.09$	$1.53^{+0.42}_{-0.34}$	1
SR7	0.07 ± 0.03	0.72 ± 0.21	$0.00^{+0.25}_{-0.00}$	0.21 ± 0.07	0.18 ± 0.08	$0.00^{+0.35}_{-0.00}$	$1.18^{+0.49}_{-0.23}$	1
SR8	$0.01^{+0.02}_{-0.01}$	0.28 ± 0.09	$0.00^{+0.25}_{-0.00}$	0.08 ± 0.04	0.05 ± 0.02	$0.00^{+0.35}_{-0.00}$	$0.42^{+0.44}_{-0.10}$	3
SR9	0.15 ± 0.05	1.93 ± 0.48	$0.06^{+0.26}_{-0.06}$	0.05 ± 0.03	0.36 ± 0.17	$0.00^{+0.35}_{-0.00}$	$2.55^{+0.67}_{-0.51}$	2
SR10	0.02 ± 0.02	0.34 ± 0.10	$0.01^{+0.25}_{-0.01}$	0.03 ± 0.02	0.02 ± 0.01	$0.31^{+0.71}_{-0.26}$	$0.72^{+0.76}_{-0.28}$	0
SR11	0.05 ± 0.02	0.38 ± 0.12	$0.00^{+0.25}_{-0.00}$	0.03 ± 0.02	0.09 ± 0.04	$0.00^{+0.35}_{-0.00}$	$0.55^{+0.45}_{-0.13}$	0
SR12	0.01 ± 0.01	0.09 ± 0.05	$0.02^{+0.25}_{-0.02}$	$0.00^{+0.01}_{-0.00}$	0.01 ± 0.01	$0.19^{+0.44}_{-0.17}$	$0.31^{+0.51}_{-0.17}$	0
SR13	0.00 ± 0.01	0.17 ± 0.06	$0.00^{+0.25}_{-0.00}$	0.02 ± 0.02	0.02 ± 0.01	$0.00^{+0.35}_{-0.00}$	$0.21^{+0.44}_{-0.13}$	0
SR14	0.11 ± 0.05	1.50 ± 0.40	$0.01^{+0.25}_{-0.01}$	1.80 ± 0.39	0.51 ± 0.15	$0.30 \pm 0.22 \pm 0.09$	$4.22^{+0.68}_{-0.63}$	5
SR15	$0.00^{+0.01}_{-0.00}$	0.24 ± 0.08	$0.00^{+0.25}_{-0.01}$	1.02 ± 0.23	0.17 ± 0.05	$0.00^{+0.35}_{-0.00}$	$1.41^{+0.50}_{-0.25}$	1

Table 5: The total expected yields in the off-Z search regions with the 2.3 fb^{-1} of data.

b-tags	H_T (GeV)	E_T^{miss} (GeV)	Expected	Observed	T1tttt ($m_{\tilde{g}}$=1000 GeV,$m_{\tilde{\chi}^0_1}$=600 GeV)	T1tttt ($m_{\tilde{g}}$=1150 GeV,$m_{\tilde{\chi}^0_1}$=100 GeV)	SR
0 b-tags	60-400	50-150	$19.26^{+4.81}_{-4.80}$	18	0.23 ± 0.06	0.00 ± 0.00	SR1
		150-300	$1.16^{+0.31}_{-0.20}$	4	0.14 ± 0.04	0.04 ± 0.01	SR2
	400-600	50-150	$1.20^{+0.47}_{-0.40}$	3	0.05 ± 0.02	0.00 ± 0.00	SR3
		150-300	$0.29^{+0.44}_{-0.09}$	0	0.06 ± 0.02	0.04 ± 0.01	SR4
1 b-tags	60-400	50-150	16.57 ± 4.52	24	0.92 ± 0.20	0.03 ± 0.01	SR5
		150-300	$2.32^{+0.80}_{-0.76}$	1	0.65 ± 0.14	0.07 ± 0.02	SR6
	400-600	50-150	$0.67^{+0.45}_{-0.09}$	2	0.25 ± 0.06	0.04 ± 0.01	SR7
		150-300	$0.48^{+0.29}_{-0.07}$	0	0.33 ± 0.08	0.09 ± 0.02	SR8
2 b-tags	60-400	50-150	$4.49^{+1.81}_{-1.79}$	4	1.12 ± 0.24	0.04 ± 0.01	SR9
		150-300	$0.31^{+0.44}_{-0.09}$	1	0.86 ± 0.18	0.08 ± 0.02	SR10
	400-600	50-150	$0.40^{+0.27}_{-0.26}$	0	0.42 ± 0.10	0.05 ± 0.02	SR11
		150-300	$0.08^{+0.43}_{-0.08}$	0	0.58 ± 0.13	0.13 ± 0.03	SR12
60-600	≥ 3 b-tags	50-300	$0.13^{+0.43}_{-0.09}$	0	2.26 ± 0.47	0.21 ± 0.05	SR13
> 600	inclusive	50-300	$1.84^{+0.44}_{-0.37}$	3	1.49 ± 0.31	1.47 ± 0.30	SR14
inclusive	inclusive	≥ 300	$1.62^{+1.22}_{-1.19}$	0	1.95 ± 0.40	3.04 ± 0.61	SR15

grounds and validates simulation for use in estimating irreducible background processes. To maximize sensitivity to a broad range of possible signal models, we investigate the 30 exclusive signal regions described in Section 6.

In the absence of any observed excesses in the data, we investigate a gluino-pair production

Table 6: The total expected yields in the on-Z search regions with the 2.3 fb^{-1} of data and signal yields for the T5qqqqWZ model for two mass points. The mass points are characterized by the mass of the $\tilde{g}$ and of the $\tilde{\chi}_1^0$ in units of GeV. The mass of the $\tilde{\chi}^{\pm}$ is fixed to $m_{\tilde{\chi}^{\pm}} = 0.5(m_{\tilde{g}} - m_{\tilde{\chi}_1^0})$.

b-tags	H_T (GeV)	E_T^{miss} (GeV)	Expected	Observed	T5qqqqWZ ($m_{\tilde{g}}$=1000 GeV,$m_{\tilde{\chi}^{\pm}}$=600 GeV)	T5qqqqWZ ($m_{\tilde{g}}$=1150 GeV,$m_{\tilde{\chi}^{\pm}}$=100 GeV)	SR
0 b-tags	60-400	50-150	38.01 ± 5.92	39	0.00 ± 0.00	6.85 ± 0.81	SR1
		150-300	$4.48^{+0.84}_{-0.75}$	3	0.82 ± 0.36	4.08 ± 0.62	SR2
	400-600	50-150	$4.88^{+1.49}_{-1.47}$	4	0.38 ± 0.19	0.86 ± 0.29	SR3
		150-300	$1.88^{+0.47}_{-0.39}$	3	0.21 ± 0.13	1.29 ± 0.36	SR4
1 b-tags	60-400	50-150	$11.84^{+2.28}_{-2.26}$	14	-	0.55 ± 0.21	SR5
		150-300	$1.53^{+0.42}_{-0.34}$	1	0.16 ± 0.16	0.49 ± 0.19	SR6
	400-600	50-150	$1.18^{+0.49}_{-0.23}$	1	0.02 ± 0.02	-	SR7
		150-300	$0.42^{+0.44}_{-0.10}$	3	0.16 ± 0.16	0.29 ± 0.15	SR8
2 b-tags	60-400	50-150	$2.55^{+0.67}_{-0.51}$	2	-	0.18 ± 0.13	SR9
		150-300	$0.72^{+0.76}_{-0.28}$	0	-	0.00 ± 0.00	SR10
	400-600	50-150	$0.55^{+0.45}_{-0.13}$	0	0.00 ± 0.00	-	SR11
		150-300	$0.31^{+0.51}_{-0.17}$	0	-	-	SR12
60-600	≥ 3 b-tags	50-300	$0.21^{+0.44}_{-0.13}$	0	-	-	SR13
> 600	inclusive	50-300	$4.22^{+0.68}_{-0.63}$	5	3.48 ± 0.65	1.01 ± 0.29	SR14
inclusive	inclusive	≥ 300	$1.41^{+0.50}_{-0.25}$	1	4.85 ± 0.81	2.37 ± 0.44	SR15

model that features cascade decays producing four top quarks in the final state. In this model, we exclude gluinos with a mass of up to 1125 GeV in the case of a massless LSP. The maximum excluded LSP mass is 650 GeV. In both masses, this represents approximately a 100 GeV improvement over exclusion limits from data collected at $\sqrt{s} = 8$ TeV.

In a bottom squark pair production model with cascade decays that contain two top quarks and two additional $W^{\pm}$ bosons, we also set limits on the masses of the bottom squark and the chargino. We exclude bottom squarks with mass of up to 550 GeV in the case of a chargino with mass of 200 GeV. The maximum excluded chargino mass is 400 GeV. In a similar search in Run-I [2], the bottom squark mass limit was slightly larger and the chargino mass limit was approximately the same.

An additional interpretation is presented in a gluino-pair production model with four light quarks and vector bosons in the final state. For the case of one W and one Z boson in the final state we exclude gluino masses up to 825 GeV for a light LSP and LSP masses up to 550 GeV for 700 GeV gluinos.

References

[1] CMS Collaboration, "Search for anomalous production of events with three or more leptons in pp collisions at $\sqrt{s} = 8$ TeV", *Phys. Rev. D* **90** (2014) 032006, doi:10.1103/PhysRevD.90.032006, arXiv:1404.5801.

[2] CMS Collaboration, "Searches for supersymmetry based on events with b jets and four W bosons in pp collisions at 8 TeV", *Phys. Lett. B* **745** (2015) 5, doi:10.1016/j.physletb.2015.04.002, arXiv:1412.4109.

[3] ATLAS Collaboration, "Search for supersymmetry at $\sqrt{s}$=8 TeV in final states with jets and two same-sign leptons or three leptons with the ATLAS detector", *JHEP* **06** (2014) 035, doi:10.1007/JHEP06(2014)035, arXiv:1404.2500.

[4] CMS Collaboration, "Performance of CMS muon reconstruction in pp collision events at sqrt(s) = 7 TeV", *JINST* **7** (2012) P10002, doi:10.1088/1748-0221/7/10/P10002, arXiv:1206.4071.

[5] CMS Collaboration, "Performance of Electron Reconstruction and Selection with the CMS Detector in Proton-Proton Collisions at vs = 8 TeV", *JINST* **10** (2015) P06005, doi:10.1088/1748-0221/10/06/P06005, arXiv:1502.02701.

[6] CMS Collaboration, "Commissioning of the Particle-Flow Reconstruction in Minimum-Bias and Jet Events from pp Collisions at 7 TeV", CMS Physics Analysis Summary CMS-PAS-PFT-10-002, 2010.

[7] CMS Collaboration, "Identification of b-quark jets with the CMS experiment", *JINST* **8** (2013) P04013, doi:10.1088/1748-0221/8/04/P04013, arXiv:1211.4462.

[8] CMS Collaboration, "Performance of b tagging at sqrt(s)=8 TeV in multijet, $t\bar{t}$ and boosted topology events", CMS Physics Analysis Summary CMS-PAS-BTV-13-001, 2013.

[9] CMS Collaboration, "Performance of the missing transverse energy reconstruction by the CMS experiment in $\sqrt{s}$ = 8 TeV pp data", (2014). arXiv:1411.0511. Submitted to *JINST*.

[10] J. Alwall et al., "The automated computation of tree-level and next-to-leading order differential cross sections, and their matching to parton shower simulations", *JHEP* **07** (2014) 079, doi:10.1007/JHEP07(2014)079, arXiv:1405.0301.

[11] T. Melia, P. Nason, R. Rontsch, and G. Zanderighi, "W+W-, WZ and ZZ production in the POWHEG BOX", *JHEP* **11** (2011) 078, doi:10.1007/JHEP11(2011)078, arXiv:1107.5051.

[12] T. Sjostrand, S. Mrenna, and P. Z. Skands, "A Brief Introduction to PYTHIA 8.1", *Comput. Phys. Commun.* **178** (2008) 852, doi:10.1016/j.cpc.2008.01.036, arXiv:0710.3820.

[13] GEANT4 Collaboration, "GEANT4—a simulation toolkit", *Nucl. Instrum. Meth. A* **506** (2003) 250, doi:10.1016/S0168-9002(03)01368-8.

[14] S. Abdullin et al., "The fast simulation of the CMS detector at LHC", *J. Phys. Conf. Ser.* **331** (2011) 032049, doi:10.1088/1742-6596/331/3/032049.

[15] W. Beenakker et al., "Production of charginos, neutralinos, and sleptons at hadron colliders", *Phys. Rev. Lett.* **83** (1999) 3780, doi:10.1103/PhysRevLett.83.3780, arXiv:hep-ph/9906298.

[16] A. Kulesza and L. Motyka, "Threshold resummation for squark-antisquark and gluino-pair production at the LHC", *Phys. Rev. Lett.* **102** (2009) 111802, doi:10.1103/PhysRevLett.102.111802, arXiv:0807.2405.

[17] A. Kulesza and L. Motyka, "Soft gluon resummation for the production of gluino-gluino and squark-antisquark pairs at the LHC", *Phys. Rev. D* **80** (2009) 095004, doi:10.1103/PhysRevD.80.095004, arXiv:0905.4749.

[18] W. Beenakker et al., "Soft-gluon resummation for squark and gluino hadroproduction", *JHEP* **12** (2009) 041, doi:10.1088/1126-6708/2009/12/041, arXiv:0909.4418.

[19] W. Beenakker et al., "Squark and gluino hadroproduction", *Int. J. Mod. Phys. A* **26** (2011) 2637, doi:10.1142/S0217751X11053560, arXiv:1105.1110.

[20] J. Butterworth et al., "PDF4LHC recommendations for LHC Run II", *J. Phys.* **G43** (2016) 023001, doi:10.1088/0954-3899/43/2/023001, arXiv:1510.03865.